# Complex Kohn approach to molecular ionization by high-energy electrons: Application to $H_2O$

Chih-Yuan Lin,[1] C. W. McCurdy,[2,1] and T. N. Rescigno[1]
[1]*Lawrence Berkeley National Laboratory, Chemical Sciences, Berkeley, California 94720, USA*
[2]*Department of Chemistry, University of California, Davis, California 95616, USA*
(Received 13 November 2013; published 9 January 2014)

The complex Kohn variational method, which has been extensively applied to low-energy molecule scattering, is extended to treat molecular ionization by fast electrons under the assumption that the incident and scattered electrons can be described by plane waves. The formulation reduces to the computation of the continuum generalized oscillation strength, which amounts to a generalization of the molecular photoionization problem to which the Kohn method has been successfully applied. To illustrate the approach, we present fully differential cross sections for the case of water, where good experimental data is available for comparison.

DOI: 10.1103/PhysRevA.89.012703 PACS number(s): 34.80.Gs

## I. INTRODUCTION

Electron-impact ionization of atoms and molecules is a fundamental collisional process which is important in a broad range of problems, from plasma physics to radiation damage in biological environments to the study of planetary atmospheres. The calculation of fully differential cross sections at low impact energies using first-principles methods is computationally challenging even for simple atomic targets. The additional complexity with molecules introduced by the multicenter nature of the problem has severely limited progress. To date, *ab initio* calculations on molecular targets using advanced nonperturbative methods have been limited to the diatomics $H_2^+$ [1,2], $H_2$ [3], and $Li_2$ [4] under the restriction that only two active electrons are explicitly treated. Calculations of differential ionization cross sections for more complex targets have all been limited to perturbative treatments where the incident, scattered, and ejected electrons are all described by distorted Coulomb or plane waves [5–7], often with simplifying assumptions aimed at making the calculations tractable [8].

In the present paper, we formulate an approach to electron-impact ionization of molecules that has been applied with some success to atomic problems [9,10]. We assume the incident electron is fast, so that extreme unequal energy-sharing collisions dominate and both the incident and scattered electrons can be treated perturbatively. However, in contrast to other perturbative treatments, we make no such assumption for the ejected electron. The interaction between the slow ejected electron and the residual molecular ion is treated by a close-coupling method and for that we employ the complex Kohn variational method [11,12], which has been very successful in previous applications to low-energy electron- molecule and electron-molecular ion scattering. The essential point we make here is that the use of a correct electron-ion scattering wave function as the final state for the ejected electron enables us to treat high-energy electron-impact ionization of molecules at the same level of sophistication achieved for atomic targets.

The theoretical formulation is presented in the following section. Section III describes our initial calculations on electron-impact ionization of water with comparisons to available experiment and the results of theoretical calculations. We conclude with a brief discussion. Atomic units are used throughout.

## II. THEORETICAL FORMULATION

We treat the collision of a "fast" ionizing electron, with initial and final momenta $\mathbf{k}_i$ and $\mathbf{k}_f$ and a neutral molecule with fixed nuclei described by a bound electronic wave function $\psi_0(\mathbf{r}_1,\ldots,\mathbf{r}_N)$. The final state consists of a "slow" ejected electron with momentum $\mathbf{k}_s$ and a molecular ion in state $\Gamma_0$ and is described by a continuum wave function $\psi^-_{\mathbf{k}_s,\Gamma_0}(\mathbf{r}_1,\ldots,\mathbf{r}_N)$. $E = k_s^2/2 + k_f^2/2$ is the energy shared by the scattered and ejected electrons and is conserved. We ignore exchange between the fast electron and the target and ejected electrons and treat only the direct interaction between the incident and target electrons. We further simplify the problem by using plane waves rather than distorted waves to describe the fast electron, i.e., we treat the fast electron in the first-Born approximation. With these assumptions, the initial and final wave functions can be written as

$$\Psi_i(\mathbf{r},\mathbf{r}_1,\ldots,\mathbf{r}_N) = \frac{1}{(2\pi)^{3/2}}\exp(i\mathbf{k}_i\cdot\mathbf{r})\psi_0(\mathbf{r}_1,\ldots,\mathbf{r}_N), \quad (1)$$

$$\Psi_f(\mathbf{r},\mathbf{r}_1,\ldots,\mathbf{r}_N) = \frac{1}{(2\pi)^{3/2}}\exp(i\mathbf{k}_f\cdot\mathbf{r})\psi^-_{\mathbf{k}_s,\Gamma_0}(\mathbf{r}_1,\ldots,\mathbf{r}_N). \quad (2)$$

The ionization amplitude can then be written as

$$f(\mathbf{k}_s,\mathbf{Q}) = \langle\Psi_f|V(r,r_1,\ldots,r_N)|\Psi_i\rangle = \frac{1}{(2\pi)^3}\langle\psi^-_{\mathbf{k}_s,\Gamma_0}|V(r,r_1,\ldots,r_N)|e^{i\mathbf{Q}\cdot\mathbf{r}}\psi_0\rangle, \quad (3)$$

where $\mathbf{Q} = \mathbf{k}_i - \mathbf{k}_f$ is the momentum-transfer vector. The triple differential cross section (TDCS) is given by

$$\frac{d\sigma}{d\Omega_f d\Omega_s dE_s} = (2\pi)^4\frac{k_f k_s}{k_i}|\langle\Psi_f|V(r,r_1,\ldots,r_N)|\Psi_i\rangle|^2. \quad (4)$$

In the first-Born approximation, the ionization amplitude only depends on the ejected electron momentum and the momentum transferred from incident to scattered electron, so for a given value of $\mathbf{k}_s$, all collisions described by combinations of $\mathbf{k}_i$ and $\mathbf{k}_f$ that give equivalent values of $\mathbf{Q}$ are described by

 

the same amplitude. The interaction potential $\mathbf{V}$ is given by

$$V(r,r_1,\ldots,r_N) = \sum_{\text{nuc}} \frac{-Z_{\text{nuc}}}{|\mathbf{r}-\mathbf{R}_{\text{nuc}}|} + \sum_{i=1,\ldots,N} \frac{1}{|\mathbf{r}-\mathbf{r}_i|}, \quad (5)$$

and the sum of the nuclear charges balances the total number of target electrons,

$$\sum_{\text{nuc}} Z_{\text{nuc}} = N. \quad (6)$$

By making use of Bethe's integral,

$$\int d^3\mathbf{r}' \frac{e^{i\mathbf{Q}\cdot\mathbf{r}'}}{|\mathbf{r}-\mathbf{r}'|} = \frac{4\pi}{Q^2} e^{i\mathbf{Q}\cdot\mathbf{r}}, \quad (7)$$

we obtain the following expression for the ionization amplitude:

$$f(\mathbf{k}_s,\mathbf{Q}) = \frac{1}{2\pi^2 Q^2} \left\langle \psi^-_{\mathbf{k}_s,\Gamma_0}(\mathbf{r}_1,\ldots,\mathbf{r}_N) \right| \times \sum_{i=1,\ldots,N} (e^{i\mathbf{Q}\cdot\mathbf{r}_i} - B) \left| \psi_i(\mathbf{r}_1,\ldots,\mathbf{r}_N) \right\rangle, \quad (8)$$

where $B$ is the complex constant

$$B = \sum_{\text{nuc}} -\frac{Z_{\text{nuc}}}{N} e^{i\mathbf{Q}\cdot\mathbf{R}_{\text{nuc}}}. \quad (9)$$

We thus obtain the well-known result that, in the Born approximation, the ionization amplitude reduces to a matrix element of a one-body operator between the initial bound state of the target and the final continuum state of ejected electron plus residual ion. Equation (8) is a generalization of the amplitude for photoionization, with the Bethe operator, $\sum_{i=1,\ldots,N}(e^{i\mathbf{Q}\cdot\mathbf{r}_i} - B)$, taking the place of the dipole operator. Ionization amplitudes with the present formalism could thus be calculated by carrying out suitable modifications to our molecular photoionization codes [13], the principal complication being that the momentum-transfer vector depends explicitly on the orientation of the molecule in the laboratory frame.

To construct an amplitude that represents an ionization process for specific values of momentum transfer and ejected electron momentum, with $\mathbf{Q}$ and $\mathbf{k}_s$ measured in the molecular body frame, we expand $\psi^-_{\mathbf{k}_s,\Gamma_0}$ in partial waves:

$$\psi^-_{\mathbf{k},\Gamma_0}(\mathbf{r}_1,\ldots,\mathbf{r}_N) = \sum_{l_0 m_0} i^{l_0} \exp(-i\delta_{l_0}) Y^*_{l_0 m_0}(\hat{\mathbf{k}}) \psi^-_{k,\Gamma_0 l_0 m_0}(\mathbf{r}_1,\ldots,\mathbf{r}_N), \quad (10)$$

with the Coulomb phase shift $\delta_{l_0}$ defined as

$$\delta_{l_0} = \arg\Gamma(l_0 + 1 - iZ/k). \quad (11)$$

Equation (8) can then be written

$$f(\mathbf{k}_s,\mathbf{Q}) = \frac{1}{2\pi^2 Q^2} \sum_{l_0 m_0} i^{l_0} \exp\left(-i\delta_{l_0}\right) Y^*_{l_0 m_0}(\hat{\mathbf{k}}_s) \left\langle \psi^-_{k_s,\Gamma_0 l_0 m_0} \right| \times \sum_{i=1,\ldots,N} (e^{i\mathbf{Q}\cdot\mathbf{r}_i} - B) |\psi_0\rangle. \quad (12)$$

In order to compare with experimental measurements of the TDCS in which the orientation of the target molecule in the laboratory frame is not determined, the computed fixed-nuclei cross sections must be averaged over all orientations of the target in the laboratory frame, keeping the angle between the ejected electron momentum and the scattered electron momentum (or equivalently, the momentum-transfer vector $\mathbf{Q}$) fixed. The averaged cross section, which is differential in the solid angles of detection for the scattered and ejected electrons, can be written

$$\frac{d\sigma^{\text{av}}}{d\Omega_{\mathbf{k}_f}\, d\Omega_{\mathbf{k}_s}\, dE_s} = (2\pi)^4 \frac{k_f k_s}{k_i} \int \frac{d\alpha\, d\,\cos\beta\, d\gamma}{8\pi^2} |f(\mathbf{k}_s(\alpha,\beta,\gamma),\mathbf{Q}(\alpha,\beta,\gamma))|^2 = (2\pi)^4 \frac{k_f k_s}{k_i} |f(\mathbf{k}_s(\alpha,\beta,\gamma),\mathbf{Q}(\alpha,\beta,\gamma))|^2_{\text{av}}, \quad (13)$$

where $\alpha$, $\beta$, and $\gamma$ are the three Euler angles required to orient the molecule in the laboratory frame. The average was carried out by numerical quadrature by evaluating the ionization amplitudes for discrete values of the Euler angles [14]. Starting with an initial value for the laboratory-frame vector $\mathbf{k}_{s_0}$ (or $\mathbf{Q}_0$), its value in the body frame for any target orientation is given by [15]

$$\mathbf{k}_s(\alpha,\beta,\gamma)[\mathbf{Q}(\alpha,\beta,\gamma)] = \begin{pmatrix} \cos\alpha\,\cos\beta\,\cos\gamma - \sin\alpha\,\sin\gamma & -\cos\alpha\,\cos\beta\,\sin\gamma - \sin\alpha\,\cos\gamma & \cos\alpha\,\sin\beta \\ \sin\alpha\,\cos\beta\,\cos\gamma + \cos\alpha\,\sin\gamma & -\sin\alpha\,\cos\beta\,\sin\gamma + \cos\alpha\,\cos\gamma & \sin\alpha\,\sin\beta \\ -\sin\beta\,\cos\gamma & \sin\beta\,\sin\gamma & \cos\beta \end{pmatrix} \mathbf{k}_{s_0}(\mathbf{Q}_0). \quad (14)$$

We found that well-converged results for the numerical average could be obtained with 10, 5, and 10 points for $\alpha$, $\cos\beta$, and $\gamma$, respectively.

A doubly differential cross section can be obtained from Eqs. (12) and (13) by integrating over the angles of $\mathbf{k}_s$ and using the orthogonality of the spherical harmonics to obtain

$$\frac{d\sigma^{\text{av}}}{d\Omega_{\mathbf{k}_f} dE_s} = \frac{4}{Q^4} \frac{k_f k_s}{k_i} \sum_{l_0 m_0} \left| \left\langle \psi^-_{k_s,\Gamma_0 l_0 m_0} \right| \sum_{i=1,\ldots,N} (e^{i\mathbf{Q}\cdot\mathbf{r}_i} - B) |\psi_0\rangle \right|^2_{\text{av}}. \quad (15)$$

The average over target orientations renders the right-hand side of Eq. (15) a function of the magnitude of $\mathbf{Q}$, but not its direction. Therefore, to obtain the singly differential, or energy-sharing, cross section, we need only integrate

over the polar angle of $\mathbf{k}_f$, integration over its azimuthal angle providing a factor of $2\pi$. We can thus write $d\Omega_{\mathbf{k}_f} = 2\pi\, Q\, dQ/k_0 k_f$ to get

$$\frac{d\sigma^{\rm av}}{dE_s} = \frac{8\pi k_s}{k_0^2 Q^3} \sum_{l_0 m_0} \int_{k_0-k_f}^{k_0+k_f} dQ \left| \langle \psi^-_{k_s,\Gamma_0 l_0 m_0} | \right. \times \sum_{i=1,\ldots,N} (e^{i\mathbf{Q}\cdot\mathbf{r_i}} - B)|\psi_0\rangle \Big|^2_{\rm av}. \quad (16)$$

The total cross section is obtained by numerically integrating the singly differential ionization cross section (SDCS) from $E_s = 0$ to $E_s = E/2$ to partially account for the indistinguishability of ejected and scattered electrons [Rudge and Seaton's Born (b) approximation [16]].

It is worth noting that if the spatial distribution of the nuclei is neglected in the interaction potential, i.e., the electron-nuclear attraction in Eq. (5) is approximated as $-N/r$, then the Bethe operator becomes $\sum_{i=1,\ldots,N}(e^{i\mathbf{Q}\cdot\mathbf{r_i}} - 1)$. This approximation to $B$ has been made in most recent perturbative treatments of molecular ionization. The constant $B$ is often dropped entirely, on the assumption that the initial bound and final continuum states are orthogonal, which is formally correct since they are both, in principle, eigenfunctions of the same Hamiltonian. However, orthogonality will generally depend on the approximations made in their respective computation. We can always ensure orthogonality by replacing $\psi^-_{\mathbf{k},\Gamma_0}$ with $\psi^-_{\mathbf{k},\Gamma_0} - \langle\psi_0|\psi^-_{\mathbf{k},\Gamma_0}\rangle\psi_0$ [17,18].

The Bethe surface, which plots the generalized oscillator strength differential (GOS) in the ejected electron energy $E$ as a function of $\ln Q^2$ and $E$, offers a useful means for displaying electron-molecule collision data within the first Born approximation over a broad range of kinematics [19]. The differential GOS, in units of inverse Rydbergs, is defined as

$$d({\rm GOS})/dE = \frac{E+I}{Q^2} \sum_{l_0 m_0} \left| \langle \psi^-_{E,\Gamma_0 l_0 m_0} | \right. \times \sum_{i=1}^{N} \exp(i\mathbf{Q}\cdot\mathbf{r}_i)|\psi_0\rangle \Big|^2_{\rm av}, \quad (17)$$

where $I$ is the binding energy of the electron being ionized and $\psi^-_{E,\Gamma_0 l_0 m_0} = \sqrt{k}\psi^-_{k,\Gamma_0 l_0 m_0}$.

We use the complex Kohn variational method to calculate $\Psi^-_f$. Since the method does not rely on single-center expansions to compute the required electron-molecular ion continuum wave functions, it is well suited to applications involving polyatomic targets. The details of the Kohn method have been previously described in the literature, so only a brief outline is given here. In the Kohn method, the wave function $\psi^-_{k,\Gamma_0 l_0 m_0}$ is expressed as

$$\psi^-_{k,\Gamma_0 l_0 m_0} = \sum_{\Gamma,l,m} \hat{A}(\chi_\Gamma F^-_{\Gamma l m,\Gamma_0 l_0 m_0}) + \sum_i d_i^{\Gamma_0}\Theta_i \equiv P\Psi + Q\Psi, \quad (18)$$

where the first sum runs over energetically open ionic states described by $(N-1)$-electron wave functions $\chi_\Gamma$ and the second sum runs over $N$-electron configuration-state functions $\Theta_i$ representing penetration and correlation terms. The operator $\hat{A}$ ensures antisymmetrization of the wave function. In the Kohn method, the momentum normalized functions $F^-_{\Gamma l m,\Gamma_0 l_0 m_0}$ are further expanded as

$$F^-_{\Gamma l m,\Gamma_0 l_0 m_0} = \sum_i c_i^{\Gamma\Gamma_0}\phi_i(r) + \sum_{lm}\sqrt{\frac{2}{\pi}}[f_l(k_\Gamma,r)\delta_{ll_0}\delta_{mm_0}\delta_{\Gamma\Gamma_0} + T^{\Gamma\Gamma_0}_{ll_0mm_0} h^-_l(k_\Gamma,r)]Y_{lm}(\hat{r})/(k_\Gamma r), \quad (19)$$

where $T^{\Gamma\Gamma_0}_{ll_0mm_0}$ are elements of the $\mathbf{T}$ matrix, $\phi_i$ is a set of orthonormal (Cartesian-Gaussian) functions, and $f_l$ and $h^-_l$ are partial-wave continuum radial functions, behaving asymptotically as regular and incoming Coulomb functions:

$$f_l(k_\Gamma, r\to\infty) \longrightarrow \sin\left(k_\Gamma r + \frac{Z}{k_\Gamma}\ln 2k_\Gamma r - \frac{\pi l}{2} + \delta_l\right),$$
$$h^-_l(k_\Gamma, r\to\infty) \longrightarrow \exp\left[-i\left(k_\Gamma r + \frac{Z}{k_\Gamma}\ln 2k_\Gamma r - \frac{\pi l}{2} + \delta_l\right)\right]. \quad (20)$$

By construction, the functions $\phi_i$ are chosen to be orthogonal to the molecular orbitals used to expand the initial target state $\Psi_i$, as are the continuum functions $f_l$ and $h^-_l$. This strong orthogonality constraint can be relaxed, if necessary, by the inclusion of appropriate penetration terms in the set $\Theta_i$. It is worth noting that all matrix elements of the one-body Bethe operator between Gaussian functions can be evaluated analytically [20]. Matrix elements of the Bethe operator between Gaussian and continuum functions are evaluated numerically using adaptive three-dimensional quadrature [12].

The present formalism provides a general framework for computing molecular ionization amplitudes in the framework of the first Born approximation for a fast incident electron. Since correlation can be included in the initial and final states, the formulation is quite general in terms of the types of collisions that can be treated, including processes such as excitation ionization, on the assumption that the incident electron energy is sufficiently high for a plane-wave treatment to be reasonable.

## III. ELECTRON-IMPACT IONIZATION OF WATER

To illustrate the previously described formalism, we consider the example of electron-impact ionization of the water molecule. Ionization cross sections for water are of fundamental interest and are widely used in the modeling of radiation damage in biological systems. Moreover, experimental measurements of the TDCS for this molecule have been carried out for an incident electron energy of 250 eV. In addition, there are other theoretical calculations using a variety of perturbative techniques available for comparison.

For this initial study, we used single-configuration wave functions to describe both the neutral target molecule and the final molecular ion states. We describe the water molecule with a self-consistent field (SCF) wave function computed in a basis of contracted Gaussian functions whose parameters are listed in Table I. For the electron-$H_2O^+$ scattering calculations, the expansion basis also included numerical continuum functions up to $l, |m| = 4$. Neutral water in its ground state has the

TABLE I. Contracted Cartesian Gaussian basis used in SCF and scattering14 calculations. Underlines separate contracted functions.

| Center | Type | Exponent | Coefficient |
|---|---|---|---|
| Oxygen | *s* | 7816.5400 | 0.002031 |
| Oxygen | *s* | 1175.8200 | 0.015436 |
| Oxygen | *s* | 273.1880 | 0.073771 |
| Oxygen | *s* | 81.1696 | 0.247606 |
| Oxygen | *s* | 27.1836 | 0.611832 |
| Oxygen | *s* | 9.5322 | 1.0 |
| Oxygen | *s* | 3.4136 | 1.0 |
| Oxygen | *s* | 0.9398 | 1.0 |
| Oxygen | *s* | 0.2846 | 1.0 |
| Oxygen | *s* | 0.095 | 1.0 |
| Oxygen | *p* | 35.1832 | 0.019580 |
| Oxygen | *p* | 7.9040 | 0.124189 |
| Oxygen | *p* | 2.3051 | 1.0 |
| Oxygen | *p* | 0.7171 | 1.0 |
| Oxygen | *p* | 0.2137 | 1.0 |
| Oxygen | *p* | 0.0737 | 1.0 |
| Oxygen | *d* | 2.0 | 1.0 |
| Oxygen | *d* | 0.85 | 1.0 |
| Oxygen | *d* | 0.32 | 1.0 |
| Oxygen | *d* | 0.128 | 1.0 |
| Hydrogen | *s* | 74.69 | 0.073771 |
| Hydrogen | *s* | 11.23 | 0.247606 |
| Hydrogen | *s* | 2.546 | 0.852933 |
| Hydrogen | *s* | 0.7130 | 1.0 |
| Hydrogen | *s* | 0.2249 | 1.0 |
| Hydrogen | *s* | 0.75 | 1.0 |

configuration $1a_1^2 2a_1^2 1b_2^2 3a_1^2 1b_1^2$. All calculations were performed at the equilibrium geometry of $H_2O$. To avoid working with nonorthogonal functions, we use a single set of molecular orbitals to construct both the initial neutral and final ion states, i.e., the final continuum states are computed in the so-called separated-channel static-exchange approximation in which the molecular ion states are described with *neutral* SCF orbitals by creating a single vacancy in one of the occupied orbitals. In this approximation, the sum over $\Gamma$ in Eq. (18) is truncated to one term for each of the considered ionization channels and $\chi_\Gamma$ is the ion state created by singly occupying one of the neutral target orbitals. The strong orthogonality constraint between the continuum function and the relevant singly occupied molecular orbital can be relaxed by including a single penetration term in $Q\Psi$, which in this case is just the neutral target state configuration. But in this frozen-core approximation, Brillouin's theorem shows that there is no nonzero matrix element connecting $P\Psi$ and $Q\Psi$, since they only differ by single excitations. Therefore, orthogonality between the initial target and final continuum states is guaranteed in this approximation and there is consequently no contribution from $B$ [Eq. (9)] in the Bethe operator.

It has been customary, in most first-Born perturbative treatments of molecular ionization, to make use of a partial-wave expansion of $e^{(i\mathbf{Q}\cdot\mathbf{r})}$ when computing the ionization cross section,

$$e^{(i\mathbf{Q}\cdot\mathbf{r})} = \sum_{l,m} 4\pi i^l j_l(Qr) Y_{lm}^*(\hat{\mathbf{Q}}) Y_{lm}(\hat{\mathbf{r}}). \tag{21}$$

We take a different approach. Since the bound initial target state as well as the square-integrable portion of the ejected electron continuum state are being expanded here in Cartesian Gaussian functions, we make use of the fact that the required bound-bound matrix elements of $e^{(i\mathbf{Q}\cdot\mathbf{r})}$ can be evaluated analytically [20]. The bound-free elements, on the other hand, we evaluate using three-dimensional adaptive quadrature.

We begin with plots of the computed Bethe surfaces for $1b_1$, $3a_1$, $1b_2$, and $2a_1$ ionization, which are shown in Fig. 1. The limiting value of $d(\mathrm{GOS})/dE$ for $Q \to 0$ gives the optical oscillator strength per unit energy $E$, which is proportional to the photoionization cross section for photon energy $E$. The other limiting case of interest for $d(\mathrm{GOS})/dE$ is where $E$ is much greater than the ionization threshold energy, which corresponds the scattering of two free electrons with the residual molecular ion acting as a spectator. For the case of free electron-electron collisions, energy and momentum conservation only allow the occurrence of the collision at $E = Q^2/2$. The peak in the Bethe surface that appears around the curve $E = Q^2/2$ forms the so-called Bethe ridge. The width of the peak along the Bethe ridge is seen to increase with decreasing ejected electron energies. The present work is focused on the kinematics of $\ln Q^2$ between $\sim$0.2 and $\sim$0.25, and energies $E$ between $\sim$0.83 and $\sim$1.6, where the electron scattering is sensitive to the electronic structure of molecular target.

Milne-Brownlie *et al.* [21] have measured TDCS for the water molecule at an asymmetric coplanar geometry for an incident electron energy of 250 eV. TDCS were measured for ionization of the $1b_1$, $3a_1$, and $1b_2$ valence molecular orbitals as well as the atomiclike $2a_1$ (carbon $2s$) orbital, whose binding energies are 12.6, 14.7, 18.5, and 32.2 eV, respectively [21]. Measurements were reported for scattered electrons detected at 15° with respect to the incident electron beam. The ejected electron signals were recorded in coincidence in the binary and recoil angular regions at a fixed energy of 10 eV for all but the $3a_1$ channel, for which the ejected electron energy was $\sim$8 eV. Milne-Brownlie *et al.* explain that the peaks in the binding energy spectrum arising from the $1b_1$ and $3a_1$ channels could not be entirely resolved and that data for the separate channels could only be obtained in the binary region. The experimental results were reported on an arbitrary scale and are not internormalized from channel to channel. Milne-Brownlie *et al.* also point out that the normalization between the binary and recoil regions was determined in a separate experiment and that the error in the binary and recoil regions ranges from 30% to 40%. We have thus normalized the experimental data to our absolute *ab initio* results to obtain the best visual fit in the binary region.

There have been several other theoretical studies—all perturbative—that compare with the Milne-Brownlie *et al.* measurements, notably the results of Champion and coworkers [6,21] and Sahlaoui and Bouamoud [22]. Unfortunately, all the published results are presented in arbitrary units. It turns out to be quite easy to modify the present complex Kohn formalism to reproduce these other Coulomb-Born (or 1CW) results. Referring to Eq. (19), which expresses the complex Kohn continuum function for the ejected electron, it is clear that by dropping all but the first term in the second sum over $l$ and $m$, we are replacing the full Kohn

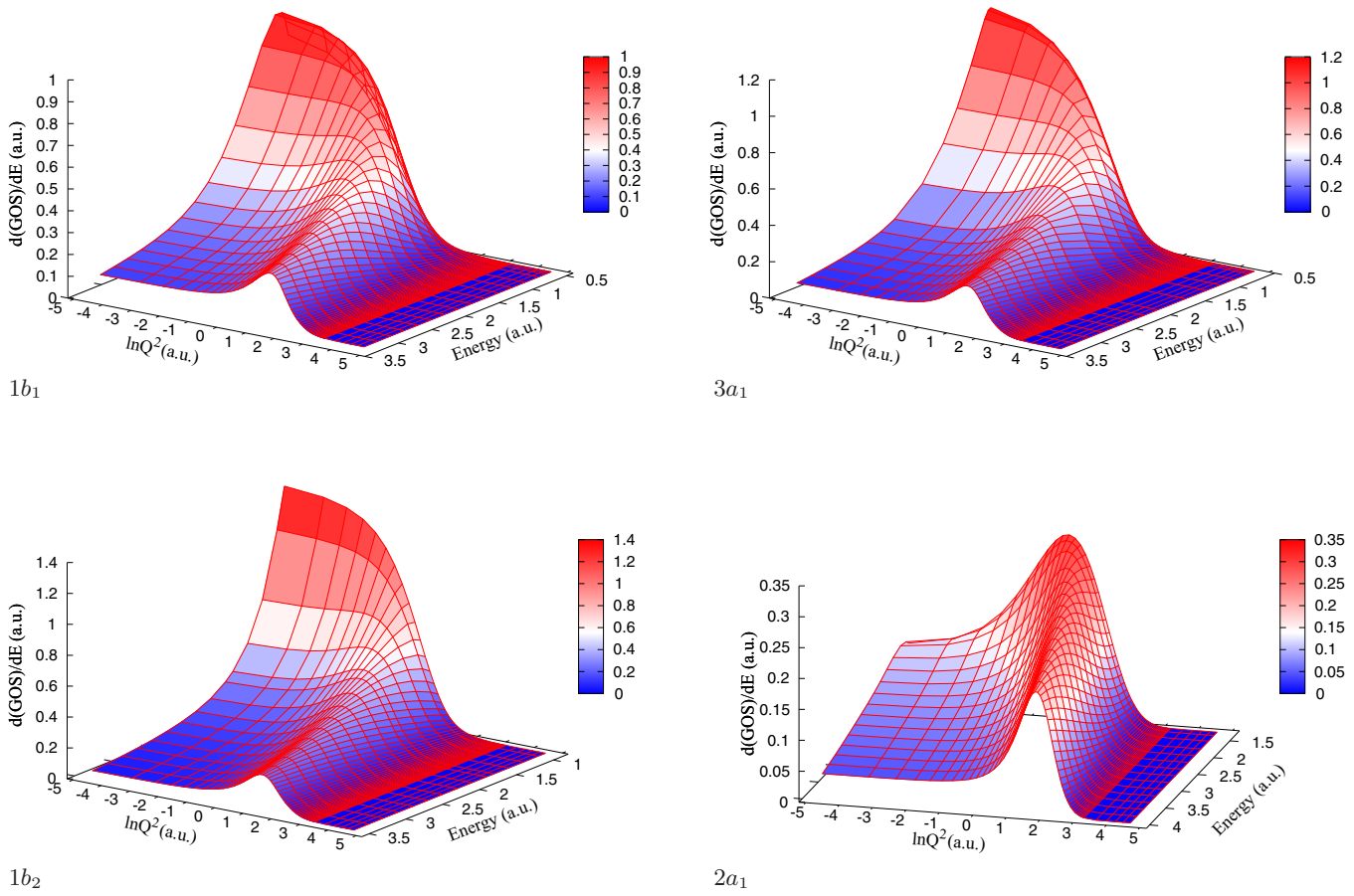


FIG. 1. (Color online) Bethe surfaces: density of differential generalized oscillator strengths, in units of $\mathrm{Ry}^{-1}$. 1 Ry = 13.6 eV.

wave function with an atomic Coulomb function. To compare with earlier calculations, we include results where the Bethe operator is taken to be $\sum_{i=1,\ldots,N} e^{i\mathbf{Q}\cdot\mathbf{r}_i}$, as was done in the original calculations reported in Refs. [5] and [21], as well as the choice $\sum_{i=1,\ldots,N}(e^{i\mathbf{Q}\cdot\mathbf{r}_i} - 1)$, which incorporates the spatially averaged electron-nuclear attraction and was used in Refs. [6] and [22]. Finally, we show results in which the atomic Coulomb function is orthogonalized to the occupied target orbital being ionized. We emphasize again that the full Kohn wave function in the separated-channel static-exchange approximation we are using is orthogonal to the target wave function.

Our calculated TDCS for the previously described kinematic conditions are shown in Fig. 2. The TDCS for $1b_1$, $3a_1$, and $1b_2$ ionization are all characterized by a double peaked structure in the binary region with local minima corresponding to the direction of the momentum transfer at 72.3°, 71.8°, and 69.6°, respectively. The three valence target orbitals all have significant oxygen $2p$ character. The TDCS for $2a_1$ orbital ionization, on the other hand, which has predominantly atomic $2s$ character, shows a single binary peak at 63.2°, as well as a shoulder between the binary and recoil regions which is consistent with experiment. The recoil region for $1b_1$ shows a single broad peak, while the $3a_1$ and $1b_2$ channels both show shallow minima in the recoil peak. This structure is also evident in the experimental data for $1b_2$ ionization. The calculated binary to recoil peak ratio agrees very well with experiment for the $2a_1$ channel, while our complex Kohn calculations give ratios for the $1b_2$ and $1b_1 + 3a_1$ cases that are somewhat smaller than the measured values.

Our Coulomb-Born results show no recoil peaks when the spatially averaged electron-nuclear attraction term is not included. This behavior had already been seen in the original 1CW results reported in Ref. [21]. The recoil peaks do appear in the 1CW results when the electron-nuclear interaction is included, as found in the results reported in Refs. [6] and [22]. The orthogonalized Coulomb-Born results also show recoil peaks in all channels, but they are significantly smaller than those found in the other calculations. We note that all the perturbative treatments give vanishingly small recoil peaks for $2a_1$ ionization. Moreover, all the perturbative results for this case had to be scaled by 0.25 to bring the magnitude of the binary peak into agreement with the complex Kohn results.

It is obvious that the momentum-transfer vector depends on the angle between the incident and scattered electron momenta. The previous calculations adopt the same kinematic conditions as the experiments with the ejected electron angle fixed at 15°. This choice results in momentum-transfer vectors of magnitude ∼1.1 a.u. for each orbital channel. In Fig. 3, we plot the TDCS, for incident and ejected electron energies fixed at 250 and 10 eV, respectively, over a wide range (0.6–2.0) of $Q$. For the $1b_1$ channel, the critical value of $Q$ which marks the onset of a splitting in the TDCS in the binary region occurs

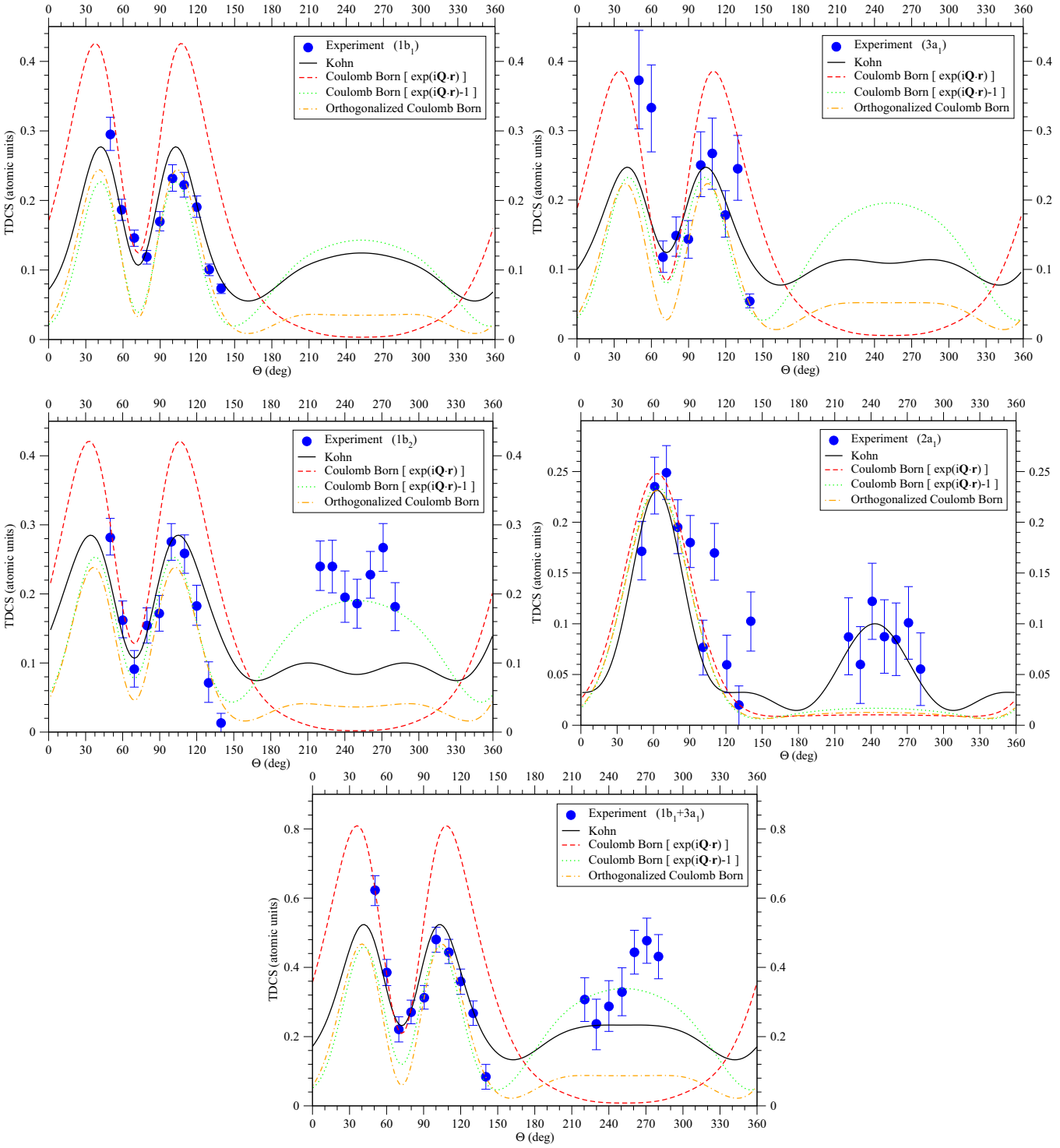


FIG. 2. (Color online) TDCS for electron-impact ionization of water. See text for description of kinematic conditions. The calculations using the complex Kohn method (solid lines) are compared with the experimental results of Milne-Brownlie *et al.* (solid circles) [21]. Unnormalized experimental data has been scaled to Kohn results to obtain the best visual fit in the binary region. Also shown are Coulomb-Born results with (dotted lines) and without (dashed lines) inclusion of electron-nuclear attraction term (see text), and Coulomb-Born results with orthogonalization to bound ionized orbital (dashed-dot lines). All theoretical data in atomic units, where 1 a.u. = 1 bohr$^2$/(sr$^2$ hartree) = $1.028 \times 10^{-18}$ cm$^2$/(sr$^2$eV). For $2a_1$ ionization, all Coulomb-Born results have been multiplied by 0.25.

near $Q = 0.7$ a.u., which is associated with a scattering angle of 9.2°. We also note that the ratio of binary to recoil peak decreases from ∼2 to ∼1 as $Q$ increases from 0.7 to 1.8. For the $3a_1$ and $1b_2$ channels, the TDCS show split binary peaks over the entire range of $Q$ plotted. The $3a_1$ and $1b_2$ channels are also characterized by a split recoil peak, which for the $1b_2$ channel disappears for values of $Q$ less than 0.8. The binary and recoil regions in the case of $2a_1$ ionization show no

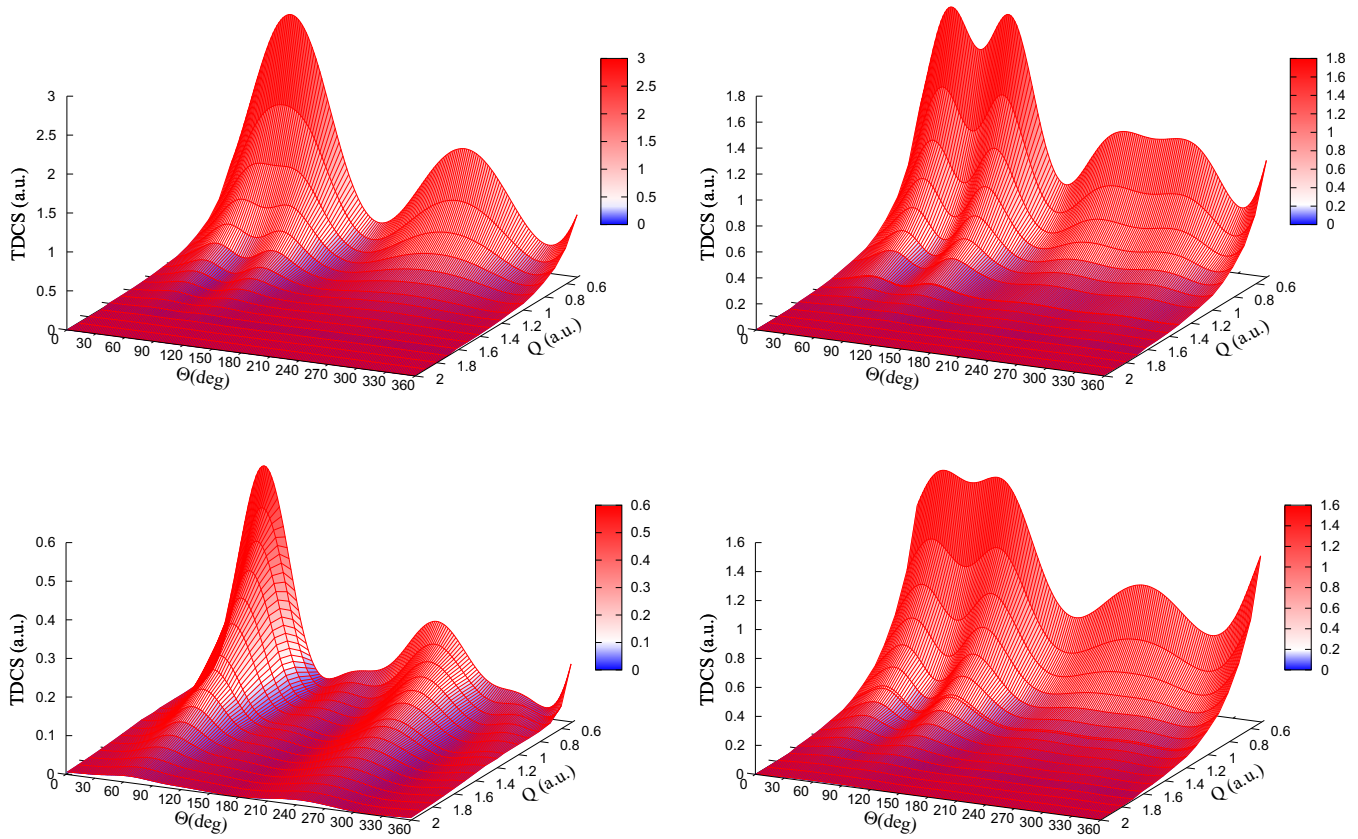


FIG. 3. (Color online) TDCS for electron-impact ionization of water as a function of ejected electron angle and $Q$. The incident and ejected electron energies are fixed at 250 and 10 eV, respectively. Results are plotted, clockwise from upper left, for $1b_1$, $3a_1$, $1b_2$, and $2a_1$ channels. Cross-section units as in Fig. 2.

splitting, but there are minor peaks on both sides of the recoil region for that case.

We have used our calculated Born amplitudes in Eq. (16) to evaluate singly differential ionization cross sections (SDCS) at 250, 500, and 1000 eV. Contributions from the $1b_1$, $3a_1$, $1b_2$, and $2a_1$ ionization channels were included in computing the SDCS. Our results are compared with experimental data [23] in Fig. 4. Agreement is good. Finally, our SDCS were numerically integrated to obtain total cross sections. The results are given in Table II, along with data from several experimental studies [23–25].

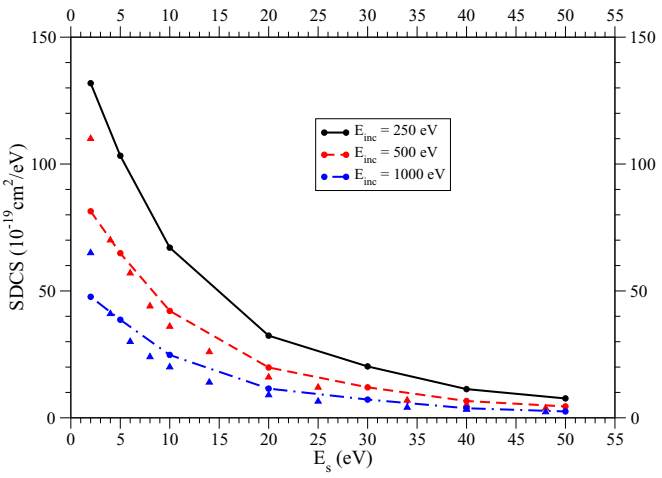


FIG. 4. (Color online) SDCS for electron-impact ionization of water. Curves with circles: calculated results; experimental results (triangles) are from Ref. [23].

## IV. DISCUSSION

We have outlined a procedure for calculating molecular ionization cross sections by fast electron impact using the complex Kohn formalism. "Fast" in the present context means that the incident and scattered electrons are sufficiently energetic for the Born approximation to be applicable. It is difficult to give a precise definition of fast since it will generally depend on the target and the process considered,

TABLE II. Total ionization cross sections (in units of $10^{-16}$ cm$^2$).

| Energy | Calculated | Experiment |
|---|---|---|
| 250 | 2.16 | 2.1[a] 2.571[b] 1.73[c] |
| 500 | 1.33 | 1.3[a] 1.713[b] 1.16[c] |
| 1000 | 0.754 | 0.78[a] 1.026[b] 0.705[c] |

[a]Bolorizadeh and Rudd (Ref. [23]).
[b]Rao, Iga, and Srivastava (Ref. [24]).
[c]Itikawa and Mason (Ref. [25]).

but it is reasonable to assume that a collision energy of 250 eV represents something of a lower limit of validity. The formalism was illustrated with calculations on the water molecule, where we find reasonably good agreement with existing experiment. For these initial illustrative studies, we have used a single-configuration SCF target wave function and the separated-channel static-exchange approximation for the final continuum channels. However, it is clear that coupled-channel calculations with correlated initial target and final ion wave functions can be accommodated using the complex Kohn formalism and we intend to examine such effects in future studies.

## ACKNOWLEDGMENTS

This work was performed under the auspices of the US Department of Energy by the University of California Lawrence Berkeley National Laboratory under Contract No. DE-AC02-05CH11231 and was supported by the US DOE Office of Basic Energy Sciences, Division of Chemical Sciences.

[1] M. S. Pindzola, F. Robicheaux, and J. P. Colgan, J. Phys. B **38**, L285 (2005).
[2] M. C. Zammit, D. V. Fursa, and I. Bray, Phys. Rev. A **87**, 020701(R) (2013).
[3] M. S. Pindzola, F. Robicheaux, S. D. Loch, and J. P. Colgan, Phys. Rev. A **73**, 052706 (2006).
[4] M. S. Pindzola, S. A. Abdel-Naby, J. A. Ludlow, F. Robicheaux, and J. Colgan, Phys. Rev. A **85**, 012704 (2012).
[5] C. Champion, J. Hanssen, and P. A. Hervieux, Phys. Rev. A **65**, 022710 (2002).
[6] C. Champion, C. Dal Cappello, S. Houamer, and A. Mansouri, Phys. Rev. A **73**, 012717 (2006).
[7] C. Kaiser, D. Spieker, J. Gao, M. Hussey, A. Murray, and D. H. Madison, J. Phys. B **40**, 2563 (2007).
[8] J. Gao, D. H. Madison, and J. L. Peacher, J. Chem. Phys. **123**, 204314 (2005).
[9] K. Bartschat and P. G. Burke, J. Phys. B **20**, 3191 (1987).
[10] A. S. Kheifets, I. Bray, and K. Bartschat, J. Phys. B **32**, L433 (1999).
[11] T. N. Rescigno, B. H. Lengsfield, and C. W. McCurdy, in *Modern Electronic Structure Theory*, edited by D. R. Yarkony (Wiley, Singapore, 1995).
[12] T. N. Rescigno, C. W. McCurdy, A. E. Orel, and B. H. Lengsfield III, in *Computational Methods for Electron-Molecule Collisions*, edited by W. M. Huo and F. A. Gianturco (Plenum, New York, 1995).
[13] T. N. Rescigno, B. H. Lengsfield III, and A. E. Orel, J. Chem. Phys. **99**, 5097 (1993).
[14] T. N. Rescigno, B. H. Lengsfield, C. W. McCurdy, and S. D. Parker, Phys. Rev. A **45**, 7800 (1992).
[15] M. E. Rose, *Elementary Theory of Angular Momentum* (World Scientific, New York, 1995).
[16] M. R. H. Rudge and M. J. Seaton, Proc. R. Soc. A **283**, 262 (1965).
[17] P. J. Marchalant, C. T. Whelan, and H. R. J. Walters, J. Phys. B **31**, 1141 (1998).
[18] P. Golecki and H. Klar, J. Phys. B **34**, L779 (2001).
[19] M. Inokuti, Rev. Mod. Phys. **43**, 297 (1971).
[20] C. W. McCurdy, Jr. and V. McKoy, J. Chem. Phys. **61**, 2820 (1974).
[21] D. S. Milne-Brownlie, S. J. Cavanagh, B. Lohmann, C. Champion, P. A. Hervieux, and J. Hanssen, Phys. Rev. A **69**, 032701 (2004).
[22] M. Sahlaoui and M. Bouamoud, Can. J. Phys. **89**, 723 (2011).
[23] M. A. Bolorizadeh and M. E. Rudd, Phys. Rev. A **33**, 882 (1986).
[24] M. Rao, I. Iga, and S. Srivastava, J. Geophys. Res. **100**, 26421 (1995).
[25] Y. Itikawa and N. Mason, J. Phys. Chem. Ref. Data **34**, 1 (2005).